Review of Scientific Instruments

# A time-to-frequency converter for measuring the shape of short optical pulses

Cite as: Rev. Sci. Instrum. **90**, 083106 (2019); https://doi.org/10.1063/1.5059553
Submitted: 20 September 2018 . Accepted: 28 July 2019 . Published Online: 19 August 2019

Brent W. Plansinis, William R. Donaldson, and Govind P. Agrawal









AIP Publishing

Review of Scientific Instruments | ARTICLE | scitation.org/journal/rsi

# A time-to-frequency converter for measuring the shape of short optical pulses

Cite as: Rev. Sci. Instrum. 90, 083106 (2019); doi: 10.1063/1.5059553
Submitted: 20 September 2018 • Accepted: 28 July 2019 •
Published Online: 19 August 2019

View Online Export Citation CrossMark

Brent W. Plansinis,[1,2] William R. Donaldson,[2,a)] and Govind P. Agrawal[1,2]

## AFFILIATIONS

[1]The Institute of Optics, University of Rochester, Rochester, New York 14627, USA
[2]Laboratory for Laser Energetics, University of Rochester, 250 E. River Road, Rochester, New York 14623, USA

[a)]**Author to whom correspondence should be addressed:** billd@lle.rochester.edu

## ABSTRACT

A time-to-frequency converter was constructed using an electro-optic phase modulator as a time lens, allowing the pulse shape in time to be transferred to the frequency domain. We used such a device to record the temporal shape of infrared pulses at a wavelength of 1053 nm (width about 7 ps) and compared these measurements to those made by using both a streak camera and an autocorrelator. This side-by-side comparison illustrates the benefits and limitations of each of the measurement methods. Numerical simulations were used to establish that our time-lens-based system can accurately measure the shape of infrared pulses between 3 ps and 12 ps. We also use our numerical model to determine how such a system can be modified to measure pulses whose width lies in the range of 1–30 ps, a range of interest for the OMEGA-EP laser at the Laboratory for Laser Energetics.



## I. INTRODUCTION

First noted in the 1960s, a mathematical equivalence exists between paraxial-beam diffraction and dispersive pulse broadening.[1–3] This equivalence, known as space–time duality, has led to the development of temporal analogs of several optical devices. An important component of such devices is the time lens,[4,5] which is designed to impose a time-dependent parabolic phase across an optical pulse passing through it, just as a traditional lens provides a parabolic phase in space. The development of such a time lens has led to applications such as temporal imaging,[4–7] spectral phase conjugation,[7] and temporal cloaking.[7,8]

Most modern time lenses produce the required parabolic phase using nonlinear effects such as four-wave mixing (FWM),[7–10] which require a highly nonlinear waveguide and a careful control of the pump dispersion and timing. Using an electro-optic phase modulator driven by a phase-locked sinusoidal radio-frequency (RF) signal, we only have to adjust the timing of our test pulse within one cycle of the RF signal, a task that can be accomplished with commercially available phase shifters. Additionally, the electro-optic phase shift does not have the intensity dependence of FWM and can be used for test pulses of any energy.[11–16] While an electro-optic modulator has been used in the past,[17] the novelty of our work is that we compare the performance of such a modulator with the measurements taken with an optical streak camera and an autocorrelator.

One of the diagnostic needs of the Laboratory for Laser Energetics (LLE) is to measure the shape of infrared ($\lambda$ = 1053 nm) pulses with durations in the range of 1–30 ps. Preshot characterization of such short-pulse beams is important to prevent damage to the system. Optical streak cameras have been used at LLE for this purpose.[18–20] However, there are several challenges to streak cameras that limit their use. First, time-of-flight broadening occurs due to variations in the kinetic energy of the generated photoelectrons. These variations in kinetic energy lead to different electron velocities, and therefore different amounts of time to reach the other end of the streak tube. For an infrared-sensitive Ag–O–Cs photocathode (denoted as S1 photocathode) used in a streak camera, this leads to impulse responses several picoseconds wide. Second, space-charge effects cause the electrons generated from short, intense pulses to repel each other. This produces broadening of the electron pulse in the drift region of the streak tube, which causes the measured pulse to be longer.[20–23] The space-charge effects can be reduced by using lower power pulses, but lower powers lead signal-to-noise to issues. The combination of these two factors means that streak cameras are not particularly well suited to measuring pulses of durations <10 ps.

Finally, and perhaps most importantly, recent experience at LLE has shown that current optical streak tubes based on S-1 photocathodes have such a limited lifetime that long-term costs of operating such streak cameras are not realistic. Therefore, it would be beneficial to develop new diagnostic techniques as alternatives to the streak cameras.

Temporal imaging systems are of particular interest because they can be run in both single-shot and averaging modes without changing the aperture and resolution of the time lens.[9] They are also well suited to imaging picosecond to tens-of-picosecond pulses.[7] In particular, electro-optic phase modulators driven by GHz-RF signals can have apertures in the tens of picoseconds. As a proof-of-concept, we have developed a pulse-imaging system that uses an electro-optic phase modulator as a time lens in a time-to-frequency converter configuration. Our device maps the pulse shape onto the spectrum, allowing the pulse shape to be recorded with an optical spectrum analyzer. In Secs. II–IV, we address the design of our system, compare its performance to a streak-camera and autocorrelator traces, and discuss how the system can be scaled up to cover a range of 1–30 ps. The comparison aspects of our work should enable appropriate decisions about which pulse measurement system to use.

## II. THEORY AND SYSTEM DESIGN

We use a time lens in a time-to-frequency conversion system in which the input pulse first propagates inside an optical fiber before passing through the time lens.[10,17,24] For a linear system, the electric field at the output of the dispersive medium of length $L$ can be related to the input electric field in the frequency domain as[25]

$$\tilde{E}_1(\omega) = \tilde{E}_0(\omega)\exp\left(\frac{i\beta_2 L}{2}(\omega-\omega_0)^2\right), \tag{1}$$

where $\tilde{E}_1(\omega)$ is the Fourier transform of the output electric field and the dispersion effects inside the fiber are included by the second derivative, $\beta_2 = d^2\beta/d\omega^2$, of the modal propagation constant $\beta$ at the central frequency $\omega_0$ of the pulse spectrum. The parameter $\beta_2$ takes into account the group velocity dispersion (GVD) and affects both the duration of input pulse and its chirp. The pulse duration and chirp after the fiber are determined by the group delay dispersion (GDD), given by $D_1 = \beta_2 L$.

When an electro-optic phase modulator driven by a sinusoidal voltage is used as a time lens, the phase shift applied to the pulse has the form

$$\Phi(t) = \phi_0\cos(2\pi\nu_m t), \tag{2}$$

where $\phi_0$ is the amplitude of the phase modulation and $\nu_m$ is the frequency of the RF signal used to drive the modulator. The phase amplitude is determined by $\phi_0 = \pi V/V_\pi$, where $V$ is the amplitude of the RF voltage used to drive the modulator and $V_\pi$ is the voltage required for the modulator to produce a phase shift of $\pi$, a known quantity for commercial modulators. The electric field after the phase modulator is then related to the electric field at the output of the dispersive medium as

$$E_2(t) = E_1(t)\exp[-i\Phi(t)]. \tag{3}$$

In close analogy to focal length of a traditional lens, a focal GDD is used to describe a time lens; it is defined as[5,26]

$$D_f = \left[(2\pi\nu_m)^2\phi_0\right]^{-1}. \tag{4}$$

For a time-to-frequency converter, the length of the dispersive medium is chosen such that the GDD of the medium, $D_1 = \beta_2 L$, is equal to the focal GDD of the time lens $D_f$.[7] Therefore, the required length in our case is $L = D_f/\beta_2$. When this condition is satisfied, the output pulse spectrum maps the temporal shape of the input pulse according to the scaling relation[10,17]

$$t = D_f(\omega-\omega_0). \tag{5}$$

As with a traditional lens, it is useful to define a time aperture and temporal resolution for our time lens. The time aperture is the longest, transform-limited Gaussian pulse that can be imaged by a time lens without significant distortion of its measured full-width at half maximum (FWHM). The time aperture for an electro-optic modulator has been previously defined in the literature and has the form[5]

$$\Delta T = \frac{1}{2\pi\nu_m}. \tag{6}$$

The time resolution is the shortest FWHM pulse duration that can be imaged by our time lens. As with the time aperture, the time resolution has been previously defined by[7]

$$\delta t = \frac{4\ln(2)}{2\pi\nu_m\phi_0}. \tag{7}$$

A schematic of the experimental setup is shown in Fig. 1. A mode-locked Yb-fiber laser (High Q femto-TRAIN IC-1053-400) producing 150-fs pulses at 1053 nm with a 38 MHz repetition rate was used as a source of optical pulses. The time lens was implemented using a high-efficiency electro-optic phase modulator designed to operate at 800 nm, but usable at 1053 nm (EOSPACE PM-5K4-10-PFU-PFU-800-LV-S). A fast photodiode (>100 MHz bandwidth) created an electronic signal of the laser pulse train, which was split into two parts with a 50/50 splitter. The first arm of the splitter was filtered with a 76 MHz bandpass filter to produce a synchronization signal at the second harmonic of the 38 MHz laser repetition rate. This 76 MHz signal matches the resonant frequency of a commercially available phase-locked dielectric resonator oscillator (PDRO), which uses phase locking to synchronize the pulse train to a high harmonic of the 76-MHz signal near 10 GHz.[27] The 10-GHz output was sent through a phase shifter to allow the timing between the 10-GHz signal and the pulse train to be adjusted so the time lens could be properly aligned. The resulting RF signal was amplified by a 33-dBm microwave amplifier and used to drive the phase modulator. This allowed our phase modulator to produce a sinusoidal phase modulation with a maximum phase amplitude of $\phi_0 = 16$ rad.

Using $\nu_m = 10$ GHz and a maximum phase amplitude of $\phi_0 = 16$ rad in Eqs. (6) and (7) gives a time aperture of $\Delta T = 15.9$ ps and a resolution of $\delta t = 2.75$ ps. The minimum focal dispersion for the time lens is then found using Eq. (4) to be $D_f = 15.8$ ps$^2$. To calibrate the time lens, we scan the sinusoidal phase modulation across the pulse using a phase shifter and adjust the amplitude of the RF voltage until the peak of the pulse spectrum oscillates over a 1.2 nm range. To create the input GDD, we used a single-mode fiber (Corning HI1060). Using the value of $\beta_2 = 23.8$ ps$^2$/km at 1053 nm, a total length of 667 m of this fiber was required to give the input dispersion of $D_1 = 15.8$ ps$^2$. The chirped pulse was then sent through the phase modulator, and the spectrum was recorded using an optical spectrum analyzer (Yokogawa AQ6370D).

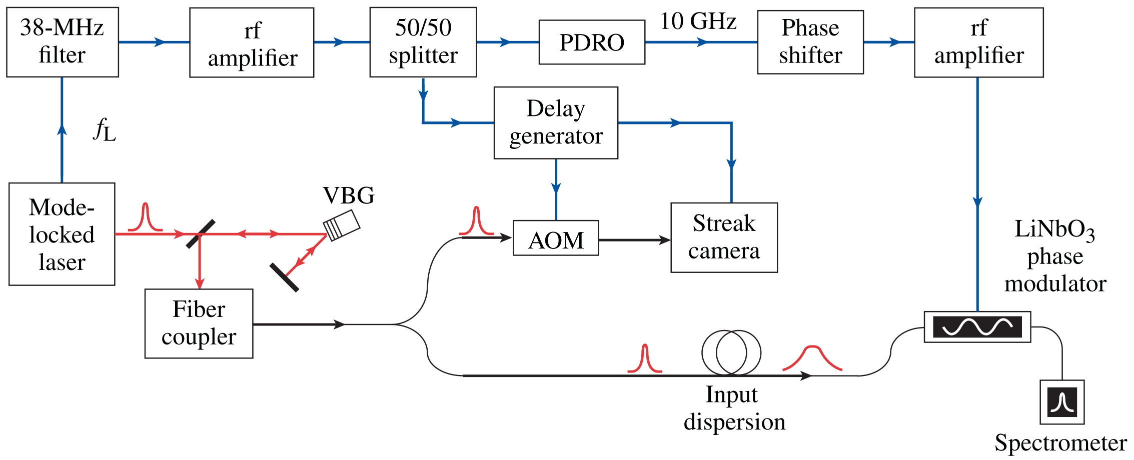


**FIG. 1**. Experimental setup for a time-to-frequency converter using a phase modulator as a time lens and an optical fiber for the input dispersion. PDRO: phase-locked dielectric resonator oscillator; AOM: acousto-optic modulator; and VBG: volume Bragg grating.

Because our laser source produces pulses shorter than the resolution of the time lens, a spectral filter needs to be applied to the laser signal to broaden the pulse in time. A volume Bragg grating (VBG) with a bandwidth of 0.5 nm was used to filter the spectrum. The VBG was used in a double-pass configuration to better attenuate the wings of the spectrum, resulting in a final spectral bandwidth of 0.254 nm.

The second arm of the RF line was filtered to 38 MHz and was used as a clock for a digital delay generator (Stanford Instruments DG645), which triggered an acousto-optic modulator (AOM) and a Rochester Optical Streak System (ROSS).[18] The AOM was used to gate the pulse train to achieve a 0.1 Hz repetition rate in order to prevent damage to the photocathode of the ROSS, and to allow only a single pulse to be captured in the streak camera image thus eliminating jitter. The ROSS was then used to capture images of the pulse shape, which are used as a comparison for the time lens measurements.

Although the time lens has a theoretical aperture of 15.9 ps, this value was found based on the FWHM of the measured pulse being largely the same as the FWHM of the actual pulse. However, even if we work with pulses shorter than the time aperture, the wings of the pulse, which extend outside of the time aperture, can still see significant distortions. To explore this effect, we performed numerical simulations of the pulse shape measured by a time-to-frequency converter with the same parameters as our experimental time lens. The input dispersion and phase modulation were modeled using Eqs. (1) and (3), respectively. The frequency axis is scaled to the time axis using the relation given in Eq. (5).

Figure 2 shows the results for Gaussian input pulses with a FWHM of (a) 15 ps, (b) 12 ps, and (c) 10 ps. The pulse shape is plotted on a logarithmic scale to better show the behavior in the pulse wings. Comparing the three plots, we see that the 12 ps and 10 ps pulses in Figs. 2(b) and 2(c) are well imaged in the wings, while the 15 ps pulse has significant errors. We can see that the wings are beginning to be distorted for the 12 ps pulse in Fig. 2(b), so our effective aperture is close to 12 ps. Note that the FWHM of the 15 ps pulse is largely unchanged, with the errors arising from a suppression of the wings. A similar problem occurs for the time resolution, with our simulations showing that the resolution is closer to $\delta t = 3$ ps.

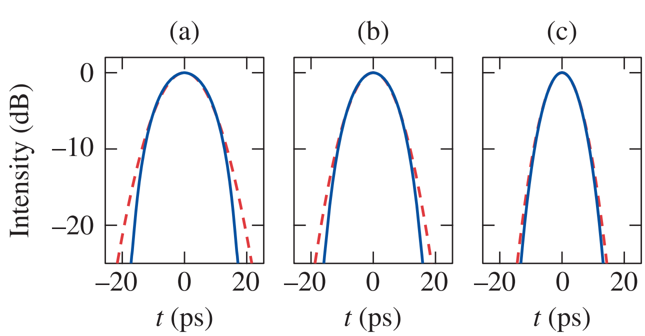


**FIG. 2**. Numerical simulations showing the pulse shape at the input (red dashed line) and the pulse shape at the output of the time-to-frequency-converter. Initial pulse widths are (a) $T_{FWHM}$ = 15 ps, (b) $T_{FWHM}$ = 12 ps, and (c) $T_{FWHM}$ = 10 ps. The time axis for the output pulse shape is obtained using the scaling from Eq. (5).

## III. EXPERIMENTAL RESULTS

Three examples of the experimentally recorded spectra are shown in Fig. 3 in the red dashed line. The wavelength axis has been converted to a time axis by first converting wavelength to frequency and then using the focal GDD, $D_f = 15.8$ ps$^2$ as a conversion factor to time. A Gaussian fit for each pulse is shown in the blue solid line, providing a measure of the FWHM duration of the pulse. These pulses should nominally have the same duration and shape, but the measured duration varies due to uncertainty in the time lens measurement and the input pulse itself. Our measurements show a typical pulse width of around 7.2 ps, with a few traces showing FWHM pulse durations near 7.32 ps as in Fig. 3(a).

We first compare these measurements to an autocorrelation trace of the pulse, as shown in Fig. 4(a). Because the autocorrelation

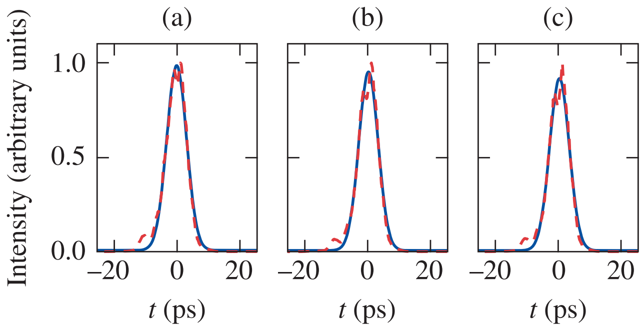


**FIG. 3**. Example measurements of the pulse shape produced by the VBG using the time-to-frequency converter (red dashed line). The time axis is obtained using the scaling from Eq. (5). A Gaussian fit to the data is shown in the blue solid line with (a) $T_{\mathrm{FWHM}}$ = 7.32 ps, (b) $T_{\mathrm{FWHM}}$ = 7.13 ps, and (c) $T_{\mathrm{FWHM}}$ = 7.24 ps.

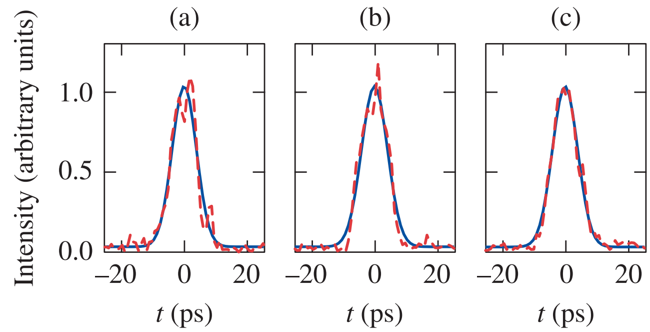


**FIG. 5**. ROSS measurements of the pulse used for generating Fig. 3 (red dashed line) and a Gaussian fit to the data (blue solid line) for three different shots. The FWHM of the calculated fits are (a) $T_{\mathrm{FWHM}}$ = 9.01 ps, (b) $T_{\mathrm{FWHM}}$ = 9.63 ps, and (c) $T_{\mathrm{FWHM}}$ = 9.38 ps.

signal was very weak due to the low peak intensity of our filtered pulses, the oscilloscope trace was averaged over 512 traces. The autocorrelation was then fitted with a Gaussian profile and found to have FWHM duration of 10.31 ps, Using the known decorrelation factor of 0.707 for Gaussian pulses, we obtain a pulse width of $T_{\mathrm{FWHM}}$ = 7.29 ps. This agrees with the FWHM calculated from the time lens measurements in Fig. 3 of 7.20 ± 0.08 ps. To obtain this value, we had to assume the input pulse shape was approximately Gaussian. While this was a good assumption in our case, the decorrelation factor can change drastically for different pulse shapes, for example, taking a value of 0.65 for sech-shape pulses. This likely explains the slight disagreement between the autocorrelation duration and the time lens measurement and is the reason why autocorrelation is not a useful technique for pulses of unknown shapes. For the time-lens technique, no assumptions need to be made for the pulse shape and, as a result, it can be used for pulses of arbitrary shapes. Finally, the pulses measured by our time lens have a small asymmetric peak located near $t = -9$ ps. This peak is likely caused by a secondary reflection in the volume Bragg grating. It is not present in the autocorrelation trace because autocorrelation involves the overlap of two copies of the same pulse, resulting in a symmetric trace. The ability of the time lens to measure asymmetries in the pulse shape is a major benefit of our technique over an autocorrelation-based technique.

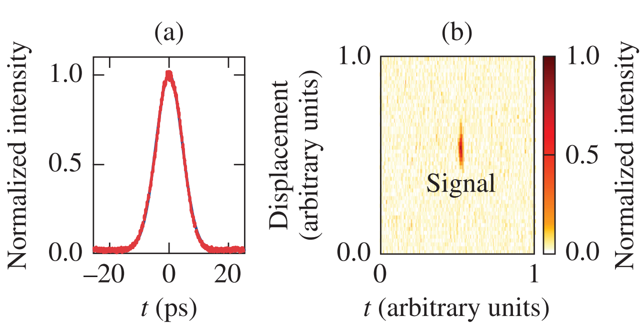


**FIG. 4**. (a) Autocorrelation of pulses used for generating Fig. 3 with a Gaussian fit with $T_{\mathrm{FWHM}}$ = 10.32 ps. (b) Streak camera image of the same pulses. The signal is labeled in the image.

We now compare our results to measurements from the ROSS. Figure 4(b) shows the image produced by the streak camera using the fastest sweep of 1.75 ns, where we have zoomed in on the region of the image corresponding to the signal pulse. Each image is averaged along the displacement axis to produce a temporal profile for a single pulse. Figure 5 shows the resulting temporal profiles from three independent streak-camera traces, using 0.85 ps/pixel for the 1.75 ns sweep. These profiles do not correspond directly to the traces in Fig. 3 but are instead used to illustrate the range of pulse durations obtained. After multiple shots, the pulse width measured on the streak camera was found to be 9.29 ± 0.76 ps, which does not agree with the 7.20 ± 0.08 ps value deduced from our time-to-frequency converter. There are several reasons behind this discrepancy. First, the signal is inherently noisier compared to other two techniques owing to the single-shot nature of the streak camera. Second, we reduced the peak power of our pulses considerably to prevent the space-charge effects, which also decreased the signal-to-noise ratio. The primary reason the streak camera measurements are consistently over a picosecond longer than those found with either the time lens or the autocorrelator is related to the time-of-flight broadening. For an impulse response $\tau$, the measured pulse width will be $T_m = \sqrt{T_0^2 + \tau^2}$. The measured impulse response of 5.78 ± 0.63 ps accounts for the observed discrepancy between the streak camera and the other two methods of measuring the pulse duration. Furthermore, even though the streak camera can potentially see the asymmetries in the pulse shape, the impulse response of the camera is longer than the asymmetry, which can no longer be resolved. Therefore, we do not see the same consistent bump in the pulse shape that could be clearly seen in the time lens measurements.

**TABLE I**. Comparison of pulse measurement techniques.

| Measurement system | Resolution (ps) | Maximum window (ps) | Pulse-shape assumption |
|---|---|---|---|
| ROSS streak camera | 5.78 | 1750 | No |
| Autocorrelator | <1 | >100 | Yes |
| Modulator time lens | 2.75 | 12 | No |
| Ultimate EP time lens | 1 | 30 | No |

## IV. CONCLUSIONS

We have built a time-to-frequency converter using an electro-optic phase modulator acting as a time lens. We used such a device to record the temporal shape of infrared pulses at a wavelength of 1053 nm (width about 7 ps) and compared these measurements to those made by using both a streak camera and an autocorrelator. Although our proof-of-concept system has successfully demonstrated the time-to-frequency conversion process, there are several improvements that must be made before its use becomes practical. The most challenging task is to expand the range of pulse durations that can be successfully imaged to cover the entire 1–30 ps range. As we saw earlier, the current time lens can image only up to 12 ps pulses accurately, so we must expand the time aperture by lowering the drive frequency, $\nu_m$. To reliably image the wings of 30-ps pulses, the drive frequency must be less than $\nu_m$ = 4 GHz, with a time aperture of $\Delta T$ = 40 ps.

By lowering the RF frequency, the time resolution will be expanded by the same factor according to Eq. (7). Therefore, the peak phase modulation must also increase by the same factor to maintain the same time resolution. However, we also wish to lower the resolution from 3 ps to 1 ps, and we must increase the amplitude of the phase modulation to $\phi_0$ = 120 rad. The first step to accomplishing this will be to use a phase modulator designed for the 1053-nm wavelength. Such modulators can produce phase amplitudes of up to $\phi_0$ = 30 rad. If we then connect four of these modulators in series, we can achieve the required phase amplitude. With the new frequency and amplitude for the time lens, the focal dispersion becomes $D_f$ = 13.2 ps$^2$, requiring only 554 m of single-mode fiber. This gives a theoretical time resolution of 0.92 ps. However, numerical simulations show that the actual resolution of the time lens is closer to 2 ps. This is likely caused by the aperture of the time lens being smaller than predicted in Eq. (6). Therefore, the resolution will actually be larger than the predicted value according to Eq. (7). Indeed, a 2 ps pulse should be well imaged by this time lens. In order to image pulses with durations down to 1 ps, the total phase amplitude would have to be doubled. This would require eight phase modulators to be connected in series, and the insertion losses would begin to affect the signal-to-noise ratio.

For the OMEGA-EP system in particular, we can work around this limitation because the longer pulses are formed by chirping a shorter pulse with diffraction gratings. Because optical fiber has the opposite GVD of the diffraction gratings, the 30-ps pulse will actually recompress during propagation through the input fiber, allowing it to fit within the aperture of the time lens. The drive frequency can therefore be increased to $\nu_m$ = 7 GHz to obtain a time aperture of $\Delta T$ = 21 ps, while keeping the phase amplitude at $\phi_0$ = 120 rad. Using these parameters, our simulations show that the full 1–30 ps range can be well imaged with only slight errors for the 1 ps pulse. Therefore, we can image much longer pulses with a considerably weaker time lens if the long pulses are properly chirped. Table I summarizes the comparison between the three measurement systems that we have employed and the proposed EP time lens. Because of its inherent symmetry, the autocorrelator cannot handle arbitrarily shaped pulses. If very long time windows are necessary, the streak camera is best but the time lens gives the best temporal resolution.

Once the time-to-frequency converter can image the proper range of pulses, the system can be converted to a single-shot mode. This can be accomplished by feeding the output of the time lens into a single-shot spectrometer. For the above system with $\nu_m$ = 7 GHz and $\phi_0$ = 120 rad, the spectrometer needs to be able to resolve spectral widths as small as 160 pm. Using a diffraction grating with a line density of 1200 g/mm and a CCD with 13.5 $\mu$m pixels, this resolution can be achieved with a spectrometer that is less than 30 cm long.

## ACKNOWLEDGMENTS

This material is based on the work supported by the Department of Energy National Nuclear Security Administration under Award No. DE-NA0001944, the University of Rochester, the New York State Energy Research and Development Authority, and the National Science Foundation under Award No. ECCS-1505636.



## REFERENCES

[1] P. Tournois, C. R. Acad. Sci. **258**, 3839 (1964).
[2] A. Papoulis, *Systems and Transforms with Applications in Optics* (McGraw-Hill, 1968), Vol. 1.
[3] S. A. Akhmanov, A. P. Sukhorukov, and A. S. Chirkin, Sov. Phys. JETP **28**, 748 (1969).
[4] B. H. Kolner and M. Nazarathy, Opt. Lett. **14**, 630 (1989).
[5] B. Kolner, IEEE J. Quantum Electron. **30**, 1951 (1994).
[6] C. Bennett and B. Kolner, IEEE J. Quantum Electron. **36**, 430 (2000).
[7] R. Salem, M. A. Foster, and A. L. Gaeta, Adv. Opt. Photonics **5**, 274 (2013).
[8] M. Fridman, A. Farsi, Y. Okawachi, and A. L. Gaeta, Nature **481**, 62 (2012).
[9] D. H. Broaddus, M. A. Foster, O. Kuzucu, A. C. Turner-Foster, K. W. Koch, M. Lipson, and A. L. Gaeta, Opt. Express **18**, 14262 (2010).
[10] A. Pasquazi, Y. Y. Park, S. T. Chu, B. E. Little, F. Légaré, R. Morandotti, J. Azaña, and D. J. Moss, IEEE J. Sel. Top. Quantum Electron. **18**, 629 (2012).
[11] J. E. Bjorkholm, E. H. Turner, and D. B. Pearson, Appl. Phys. Lett. **26**, 564 (1975).
[12] T. Kobayashi, H. Yao, K. Amano, Y. Fukushima, A. Morimoto, and T. Sueta, IEEE J. Quantum Electron. **24**, 382 (1988).
[13] B. H. Kolner, Appl. Phys. Lett. **52**, 1122 (1988).
[14] A. A. Godil, B. A. Auld, and D. M. Bloom, Appl. Phys. Lett. **62**, 1047 (1993).
[15] M. T. Kauffman, A. A. Godil, B. A. Auld, W. C. Banyai, and D. M. Bloom, Electron. Lett. **29**, 268 (1993).
[16] A. A. Godil, B. A. Auld, and D. M. Bloom, IEEE J. Quantum Electron. **30**, 827 (1994).
[17] M. T. Kauffman, W. C. Banyai, A. A. Godil, and D. M. Bloom, Appl. Phys. Lett. **64**, 270 (1994).
[18] W. R. Donaldson, R. Boni, L. Keck, and P. Jaanimagi, Rev. Sci. Instrum. **73**, 2606 (2002).
[19] R. Lerche, J. W. McDonald, R. L. Griffith, G. Vergel de Dios, D. S. Andrews, A. W. Huey, P. M. Bell, and O. L. Landen, Rev. Sci. Instrum. **75**, 4042 (2004).
[20] J. Qiao, P. Jaanimagi, R. Boni, J. Bromage, and E. Hill, Rev. Sci. Instrum. **84**, 073104-1 (2013).

[21] B.-L. Qian and H. E. Elsayed-Ali, J. Appl. Phys. **91**, 462 (2001).
[22] B. J. Siwick, J. R. Dwyer, R. E. Jordan, and R. J. D. Miller, J. Appl. Phys. **92**, 1643 (2002).
[23] A. Verna, G. Greco, V. Lollobrigida, F. Offi, and G. Stefani, J. Electron Spectrosc. Relat. Phenom. **209**, 14 (2016); e-print arXiv:1603.08581.
[24] M. A. Foster, R. Salem, and A. L. Gaeta, Opt. Photonics News **22**, 29 (2011).
[25] G. P. Agrawal, *Nonlinear Fiber Optics*, 5th ed. (Elsevier, Amsterdam, 2013).
[26] B. H. Kolner, J. Opt. Soc. Am. A **11**, 3229 (1994).
[27] I. Kang, C. Dorrer, and F. Quochi, Opt. Lett. **28**, 2264 (2003).